Acta Biomaterialia 9 (2013) 4744–4753

Contents lists available at SciVerse ScienceDirect

Acta Biomaterialia

journal homepage: www.elsevier.com/locate/actabiomat

A high poly(ethylene glycol) density on graphene nanomaterials reduces the detachment of lipid–poly(ethylene glycol) and macrophage uptake

Mei Yang [a,b], Momoyo Wada [b], Minfang Zhang [b], Kostas Kostarelos [c], Ryota Yuge [d], Sumio Iijima [a,b,d], Mitsutoshi Masuda [b,*], Masako Yudasaka [b,*]

[a] Department of Material Science and Engineering, Meijo University, 1-501 Shiogamaguchi, Tenpaku, Nagoya 468-8502, Japan
[b] Nanotube Research Center, National Institute of Advanced Industrial Science and Technology, 5-2, 1-1-1 Higashi, Tsukuba 305-8565, Japan
[c] Nanomedicine Laboratory, Center for Drug Delivery Research, The School of Pharmacy, University of London. 29-39 Brunswick Square, London WC1N 1AX, UK
[d] NEC Corporation, 34 Miyukigaoka, Tsukuba, Ibaraki 305-8501, Japan

ARTICLE INFO

Article history:
Received 16 March 2012
Received in revised form 26 August 2012
Accepted 11 September 2012
Available online 17 September 2012

Keywords:
Single-walled carbon nanohorn
Noncovalent functionalization
Lipid–poly(ethylene glycol)
Detachment
Macrophage uptake

ABSTRACT

Amphiphilic lipid–poly(ethylene glycol) (LPEG) is widely used for the noncovalent functionalization of graphene nanomaterials (GNMs) to improve their dispersion in aqueous solutions for biomedical applications. However, not much is known about the detachment of LPEGs from GNMs and macrophage uptake of dispersed GNMs in relation to the alkyl chain coverage, the PEG coverage, and the linker group in LPEGs. In this study we examined these relationships using single walled carbon nanohorns (SWCNHs). The high coverage of PEG rather than that of alkyl chains was dominant in suppressing the detachment of LPEGs from SWCNHs in protein-containing physiological solution. Correspondingly, the quantity of LPEG-covered SWCNHs (LPEG-SWCNHs) taken up by macrophages decreased at a high PEG coverage. Our study also demonstrated an effect of the ionic group in LPEG on SWCNH uptake into macrophages. A phosphate anionic group in the LPEG induced lower alkyl chain coverage and easy detachment of the LPEG, however, the negative surface charge of LPEG-SWCNHs reduced the uptake of SWCNHs by macrophages.

1. Introduction

Graphene nanomaterials (GNMs), including graphene, carbon nanotubes, and carbon nanohorns, have found many potential biological applications and have been acknowledged as next generation novel drug delivery nanocarriers [1–6]. The practical implementation of GNM-based nanocarriers has been greatly facilitated by various dispersion techniques [7,8], such as covalent or non-covalent functionalization with polymers [9–11], biological macromolecules[12,13], and amphiphilic molecules [14,15]. Covalent functionalization methods usually involve a harsh pre-oxidation that disrupts the π-electron networks of the GNMs. Non-covalent functionalization, especially using poly(ethylene glycol)-based amphiphilic lipids (LPEGs), has been widely adopted as an effective and simple to handle protocol to yield water-soluble GNMs [16–19].

Non-covalent functionalization of LPEG onto GNMs not only improves the solubility of GNMs, but also inhibits the binding of plasma proteins and the recognition of GNMs by macrophages [20,21], thereby prolonging the blood circulation of GNMs, which would be an advantage for anticancer therapy [22,23]. Like many surfactants, non-covalently adsorbed LPEG may, however, gradually detach from the GNM surface [24] and the exposed hydrophobic region becomes accessible to serum proteins. Consequently, serum-mediated recognition of GNMs by phagocytic cells of the reticuloendothelial system may yield a short blood circulation lifespan or decrease the potential targeting effect of GNMs [25]. Therefore, investigation of the detachment of LPEGs from GNM surfaces and macrophage uptake of LPEG-covered GNMs will guide us in the selection of appropriate LPEGs for GNMs for in vivo drug delivery. No research to has date tried to elucidate the relationship between PEG coverage density and detachment of LPEGs from GNM surfaces or the macrophage uptake of LPEG-covered GNMs.

To quantitatively establish such relationships spherical aggregates of about 2000 single-walled carbon nanohorns (SWCNHs) (Fig. 1) were used as the model GNM because of their extremely hydrophobic surface and the large quantities available without the use of a metal catalyst [26]. The SWCNHs were solubilized with two commercially available LPEGs and five synthetic LPEGs (Table 1). These LPEGs with different alkyl chains, different PEG chain lengths, and linkers were designed in an effort to determine the effect of different chemical structures on the dispersion ability. By quantitatively measuring the amounts of LPEG using a colorimetric method we were able to determine the saturated absorption of LPEGs on SWCNHs, from which the alkyl chain

* Corresponding authors. Tel.: +81 29861 9368; fax: +81 9313 4545 (M. Masuda), tel./fax: +81 29861 6290 (M. Yudasaka).
E-mail addresses: m-masuda@aist.go.jp (M. Masuda), m-yudasaka@aist.go.jp (M. Yudasaka).

1742-7061/$ - see front matter © 2012 Acta Materialia Inc. Published by Elsevier Ltd. All rights reserved.
http://dx.doi.org/10.1016/j.actbio.2012.09.012

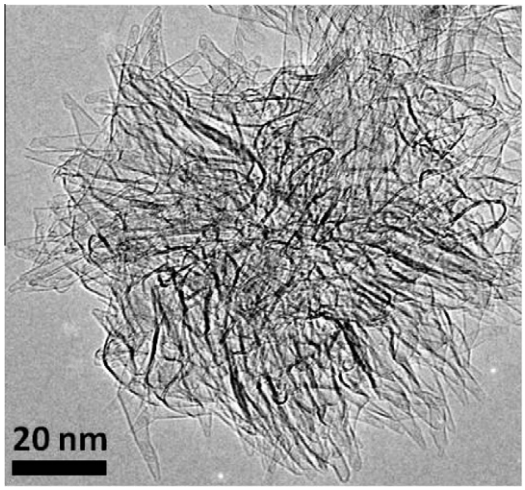

Fig. 1. Transmission electron microscope image of a SWCNH aggregate.

coverage and PEG coverage density were calculated for each LPEG-covered SWCNHs (LPEG-SWCNH). Further, for the first time, these coverage densities were correlated with dispersion ability, dispersion stability, detachment of LPEGs from SWCNHs, and macrophage uptake of LPEG-SWCNH. It was found that when either the alkyl chain coverage or the PEG coverage density exceeded a certain value the SWCNHs were finely dispersed; a higher PEG coverage density resulted in less detachment of LPEGs from SWCNHs and lower macrophage uptake of LPEG-SWCNH. Finally, the low acute toxicity of LPEG-SWCNH was confirmed with macrophages.

2. Materials and methods

2.1. Materials and measurements

The SWCNHs used in this study were produced by CO_2 laser ablation of graphite in an argon atmosphere (1 atm) without using metal catalysts, as described previously [26]. The purity of the SWCNHs produced was estimated to be 95%, with 5% giant graphite ball impurities [27,28]. N-Palmitoyl-sphingosine-1-[succinyl(methoxypolyethylene glycol) 2000] (C-PEG) and 1,2-distearoyl-sn-glycero-3-phosphoethanolamine-N-[methoxy(polyethylene glycol) 2000], ammonium salt (D-PEG) were purchased from Avanti. For the synthesis stearoyl chloride and dodecanoyl chloride (TCI, Japan), solvents (Wako, Japan), and polyethylene glycols of the highest grade were purchased and used without purification. Proton nuclear magnetic resonance (^{1}H NMR) spectra were recorded using an Avance 400 (400 MHz at 23 °C) spectrometer. Chemical shift values (δ) are given in parts per million using tetramethyl silane (^{1}H NMR, δ_H = 0.00 in $CDCl_3$) as an internal standard. Preparative column chromatography was performed on silica gel. The chromatographic purity of the intermediates was monitored by thin layer chromatography (Kiesel gel F254, Merck).

Table 1
Chemical structures of LPEGs.

Name	Structure	Molecular weight
Double alkyl chain		
C-PEG	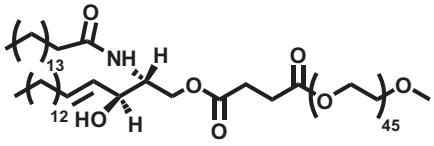	2634.4
D-PEG	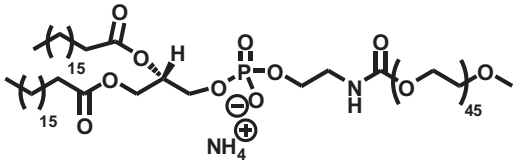	2805.5
Single alkyl chain		
C18E114[a]	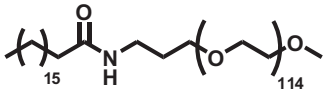	5324.6
C18E45[a]	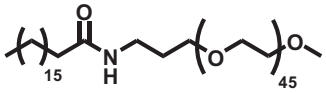	2324.6
C18E114-ester[a]	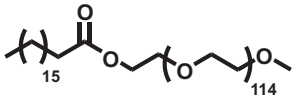	5311.5
E45C20E45[a]	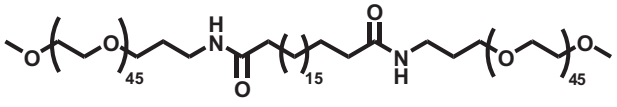	4422.7
C10E45[a]	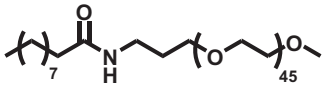	2212.4

[a] The C*n* and E*m* in C*n*E*m* refers to the carbon numbers in the alkyl chain and the ethylene glycol repeated units in the PEG chain.

2.2. Synthesis

2.2.1. Synthesis of C18E114

A dichloromethane solution (0.5 ml, anhydrous) of stearoyl chloride (48 mg, 0.16 mmol) was added dropwise into a dichloromethane solution (2 ml, anhydrous) of α-aminopropyl-ω-methoxypolyethyleneglycol (molecular weight 5000 Da, 500 mg, 0.10 mmol, Sunbright MEPA-50H, NOF Corp., Japan) and triethylamine (28 μl, 0.20 mmol) at 0 °C. The solution was stirred at the same temperature for 1 h, and then at room temperature for 3 h. The condensation reaction was quenched with water and the solvent evaporated. The residue was dissolved in methanol, neutralized with ion exchange resin (Amberlite, IRA400J, Organo, Japan), and subjected to silica gel column chromatography (elution with chloroform/methanol 90:10 vol.%) and size exclusion chromatography (elution with methanol, Toyopearl HW-40S, Tosoh Bioscience, Japan). Solvent evaporation of the fractions gave C18E114 as an amorphous solid (493 mg, 94%): $R_f = 0.3$ (chloroform/methanol 90:10 vol.%); ^{1}H NMR (in $CDCl_3$) δ 3.44–3.84 (m, 460H, O–CH_2–CH_2–, –CH_2–NH), 3.38 (s, 3H, OCH_3), 2.14 (t, J = 8.0 and 7.3 Hz, 2H, –CH_2–CO), 1.76 (m, 2H, –CH_2–CH_2–NH), 1.61 (m, 2H, –CH_2–CH_2–CO), 1.25 (m, 28H, –CH_2–), 0.88 (t, J = 7.0 and 6.6 Hz, 3H, –CH_3).

2.2.2. Synthesis of other LPEGs

C18E45, C18E114-ester, E45C20E45, and C10E45 were prepared by a similar procedure to that of C18E114. Details are provided in Supplementary information.

2.3. Measurement of LPEG adsorption on SWCNHs

A series of LPEG solutions (0.004, 0.01, 0.02, 0.04, and 0.1 mg ml^{-1}) were prepared by the dilution of a stock solution, which was prepared by dissolving the LPEG powder in MilliQ water at room temperature. 0.2 mg of SWCNHs were dispersed in 10 ml of each of the LPEG solutions, after which the mixtures were sonicated using a bath sonicator for 10 min and stirred at 600–700 r.p.m. over 17 h. The non-adsorbed LPEGs were filtered out using a 0.1 μm syringe-driven filter (Millipore) (see Supplementary information, Table S1 for LPEG recovery). The concentrations of the non-adsorbed LPEGs were determined using the modified Dragendorff reagent method reported previously [29]. Briefly, 0.5 ml of purified water, 1.5 ml of 0.05 N HCl, and 0.5 ml of Dragendorff reagent were added to 2.5 ml of each filtrate. The Dragendorff reagent chelates with the PEG chain and forms an orange colored solution. After 15 min the UV absorption at 510 nm was determined using a UV–vis-NIR spectrometer (Lambda 19, PerkinElmer Japan). Thus, the free LPEG concentration could be calculated using a calibration curve prepared under the same conditions.

2.4. Particle size measurement of dispersed SWCNHs

SWCNHs (0.20 mg) were added to 10 ml of phosphate-buffered saline (PBS) (pH 7.4), each of which contained 0.10 mg ml^{-1} of a different LPEG. The suspensions were shaken and sonicated using a bath sonicator for 10 min. After sonication dynamic light scattering (DLS) (FPAR-1000, Otsuka Electronics, Japan) measurements were conducted at 25 °C to measure the size of the dispersed SWCNHs.

2.5. Measurement of dispersion stability

To evaluate the dispersion stability of the SWCNHs in the different LPEG solutions the light transmittance of the SWCNH dispersions was measured as a function of time at 700 nm for nine consecutive days using a UV–vis-NIR spectrometer (Lambda 19, PerkinElmer Japan). Dispersions of SWCNHs (0.02 mg ml^{-1}) in PBS were prepared by strong shaking followed by 10 min sonication with 0.10 mg ml^{-1} of each of the different types of LPEG.

2.6. Measurement of LPEG detachment from SWCNHs

As indicated above, 5 mg of SWCNHs were dispersed in 250 ml of water containing C-PEG, D-PEG, C18E114, or C18E45 (0.1 mg ml^{-1}). The non-adsorbed LPEGs were removed by filtration through 0.2 μm filters (Whatman) using a vacuum pump, and the LPEG-SWCNH residues were then redispersed in 3 ml of purified water and added to 12 ml of PBS supplemented with bovine serum (50% bovine serum). The mixtures were incubated at 37 °C for 0, 24, and 48 h. At each time point 1 ml of the solution was removed and passed through 0.1 μm syringe-driven filters (Millipore) to collect the detached LPEGs (see Supplementary information, Table S2 for LPEG recovery). To determine the LPEG concentrations in bovine serum-supplemented PBS excess methanol was added to the filtrates to separate the proteins. After centrifugation at 12,000 r.p.m. for 10 min at room temperature the supernatant was sampled and the LPEG concentration was measured using the Dragendorff reagent method.

2.7. Macrophage uptake of LPEG-SWCNH

The SWCNHs (2 mg) were dispersed in 4 ml of C-PEG, D-PEG, C18E114, and C18E45 water solutions (2.5 mg ml^{-1}). In order to remove the free LPEGs each dispersed SWCNH solution was centrifuged with a 0.1 μm centrifugal filter (Millipore) at 12,000 r.p.m. for 15 min at room temperature. The SWCNHs were redispersed in the cell medium described below and their concentration recalculated to 10 μg ml^{-1} based on the visible light absorption of the SWCNHs at 700 nm. Murine RAW264.7 macrophages (ECACC) were cultured as a monolayer at 37 °C in a humidified atmosphere with 5% CO_2 in RPMI medium 1640 (GIBCO) containing 10% fetal bovine serum (GIBCO) supplemented with penicillin at 5 U ml^{-1} and streptomycin at 5 μg ml^{-1} (GIBCO). Prior to addition of the SWCNH dispersions RAW264.7 cells were seeded in 35 mm glass based dishes at a density of 1.6×10^5 cells ml^{-1} in culture medium (3 ml) and incubated for 24 h. Then the culture medium was replaced by 3 ml of the C-PEG, D-PEG, C18E114, and C18E45 SWCNH dispersions as described above (SWCNH concentration 10 μg ml^{-1}) and incubated for 24 and 48 h. After incubation the culture medium was removed and the cells were rinsed twice with PBS in order to remove the free LPEG-SWCNH and those bound to cell surfaces. The cells were visualized using confocal microscopy (LSM 5 Pascal, Zeiss). The numbers of intracellular SWCNHs were analyzed using a previously reported method [30]. Briefly, the cells were washed twice with PBS and then detached from the culture dishes by adding 0.25% trypsin–EDTA (Sigma). After counting the number of cells using a hemocytometer under an optical microscope, the cell suspension was centrifuged at 120g for 5 min. The cell pellets were resuspended in 1% Triton X-100 (Sigma) in water and sonicated into lysates for 20 min with a horn sonicator (~300 W). The optical absorbance of the SWCNHs in the cell lysates were measured at 700 nm and the concentration of SWCNHs in the lysates were calculated based on a calibration curve. The quantities taken up were determined as:

$$\text{cellular uptake(ng cell}^{-1}) = (\text{concentration of SWCNHs(ng ml}^{-1}) \times \text{volume(ml)})/\text{number of cells}$$

2.8. Assessment of cytotoxicity

The cytotoxicity of the LPEG-SWCNHs was determined using the cell proliferation reagent WST-1 (Roche) and protein assay (Bradford method) in RAW264.7 (ECACC) cells. For the WST-1

assay cells (3.8×10^5 cells ml^{-1}) were seeded in a 96-well plate with a final volume of 100 μl well^{-1} culture medium. After 24 h the culture medium was replaced by 100 μl of LPEG-SWCNH culture medium solution (LPEG-SWCNH concentration 1–100 μg ml^{-1}). After incubation for 24 and 48 h at 37 °C the culture medium was removed and the cells were rinsed twice with PBS. Then 100 μl of culture medium containing 10 vol.% WST-1 reagent was added to each well. The absorbance of WST-1-derived formazan was measured using a microplate reader (Model 680, Bio-Rad, Japan) at 450 nm with the reference wavelength set at 620 nm. The relative cell viability was calculated using the equation:

$$(A_{\text{experimental}} - A_{\text{blank}})/(A_{\text{control}} - A_{\text{blank}}) \times 100\%$$

in which A_{blank} is the absorbance of cell medium containing WST-1 and A_{control} is the absorbance of cells without SWCNH treatment.

For protein assay the cells (3.6×10^5 cells ml^{-1}) were seeded in a 24-well plate with a final volume of 1 ml well^{-1} culture medium. After 24 h the culture medium was replaced by 1 mL of LPEG-SWCNH culture medium solution (LPEG-SWCNH concentration 1–100 μg ml^{-1}). After incubation for 24 and 48 h at 37 °C the medium was removed and the cells were rinsed twice with PBS, followed by lysis with celLytic-M (Sigma) containing a protease inhibitor cocktail (Nacalai). The lysate was centrifuged at 18,000*g* for 10 min at 4 °C to remove SWCNH. 10 μl of the supernatant was added to a 96-well plate together with 250 μl of Bradford reagent (Sigma). The plates were incubated at room temperature for 10 min and the optical absorbance (595 nm) was measured using a plate reader (Synergy2, BioTek). The relative quantity of protein was calculated by comparison with a control cell without LPEG-SWCNH treatment.

2.9. Statistical analysis

The results are shown as the average values of double independent experiments or expressed as the means ± standard deviation (SD) of independent experiments ($n \geqslant 3$). Statistical analysis was performed using Prism software (GraphPad software Inc.). The data were analyzed by a one-way analysis of variance followed by Dunnett's test. $P < 0.05$ was considered significant.

3. Results and discussion

3.1. Quantity of LPEGs adsorbed and surface coverage on SWCNHs in water

The amount of LPEG adsorbed was measured using the Dragendorff reagent method [29], as described above. Fig. 2a shows that the amount of LPEG on the SWCNHs increased with an increase in the LPEG/SWCNH ratio, with the adsorption becoming saturated at a weight ratio of 5:1, except for C-PEG and C18E114.

It is generally considered that LPEG amphiphiles can disperse carbon nanoparticles in aqueous solution, with the hydrophobic domains attached to the GNM surface via van der Waals forces and hydrophobic effects and with the PEG chain stretching out into the aqueous medium [31]. We estimated the surface area coverage of the LPEGs on the SWCNHs from the amount adsorbed at an initial weight ratio of 5 g g^{-1} (LPEGs/SWCNHs). In the calculation we assumed monolayer attachment of the alkyl chains on the SWCNH surface and extension of the PEG chains into the aqueous medium (Fig. 2b). On the basis of atomic force microscopy and neutron scattering studies on alkyl chains deposited on graphite [32–34] the areas of alkyl chains adsorbed on the SWCNHs were: $C_{18}H_{37}$, 1.00 nm^2; $C_{15}H_{31}$, 0.83 nm^2, $C_{10}H_{21}$, 0.56 nm^2. The surface area of the as-grown SWCNHs was 308 m^2 g^{-1} [35]. Thus the percentage surface area coverage by alkyl chains and the PEG chain density can be calculated using the formulae:

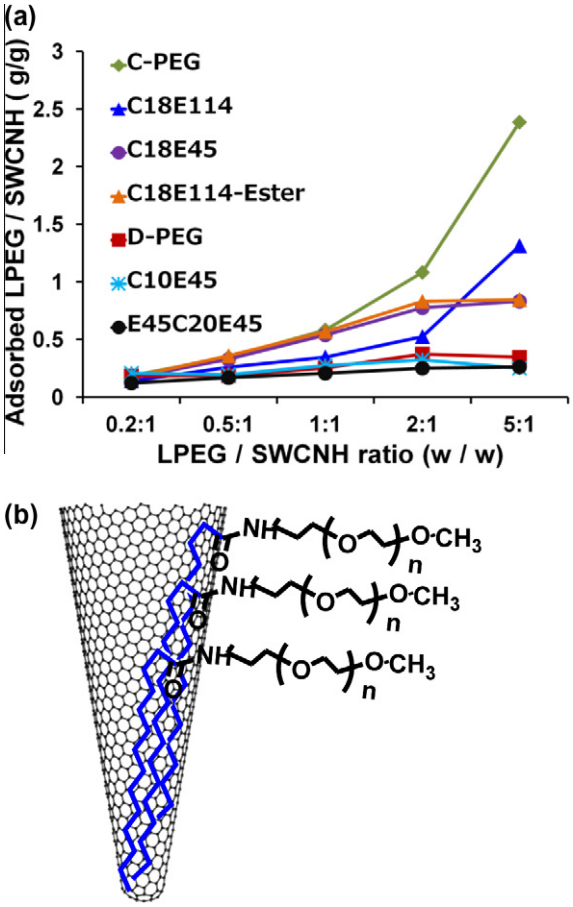

Fig. 2. (a) Amounts of LPEGs adsorbed on SWCNHs. Data were presented as average values of double independent experiments. (b) Schematic illustration to show that the alkyl chain was adsorbed on the SWCNH surface, while the PEG chains stretched into the aqueous medium. (This does not show the actual adsorption morphology.)

$$\text{alkyl chain coverage } (\%) = (\text{amount adsorbed per g SWNHs} \times 6.02 \times 10^{23} \times \text{alkyl chain area})/(\text{molecular weight} \times 308 \times 10^{18}) \times 100\%$$

$$\text{PEG coverage density } (\text{ng cm}^2) = (\text{amount adsorbed per g SWNHs} \times 10^9 \times \text{molecular weight of PEG chain})/(\text{molecular weight of LPEG} \times 308 \times 10^4)$$

The calculated alkyl chain coverage and PEG coverage density values are listed in Table 2.

In general the alkyl chain coverage of LPEGs on the SWCNHs depended largely on the chemical structures of the LPEGs, e.g. the alkyl chain and PEG chain lengths. Comparing the double alkyl chain LPEGs, D-PEG had an alkyl chain coverage and PEG coverage density that were much lower than those of C-PEG. This suggests that the electrostatic repulsive force between the anionic phosphate groups in D-PEG may decrease its grafting density on SWCNHs [19,36,37]. The alkyl chain coverage of C-PEG on the SWCNHs was exceptionally high, close to 300%, which suggests that C-PEG might form multiple layers on the SWCNH surface. In the single alkyl chain group, C18E114, C18E114-ester, and C18E45 presented high alkyl chain coverages (30–70%) and high PEG coverage densities (200–400 ng cm^{-2}), while C10E45 and E45C20E45 had low alkyl chain coverages of 12–13% and PEG coverage densities of 70–80 ng cm^{-2}.

Table 2
Surface area coverage of LPEGs on SWCNHs at a LPEG:SWCNH ratio of 5:1.

	C-PEG	D-PEG	C18E114	C18E45	C18E114-ester	E45C20E45	C10E45
Amount attached ($g\,g^{-1}$)	2.385	0.345	1.312	0.831	0.845	0.263	0.251
Alkyl chain coverage (%)	294	48	48	70	31	13	12
PEG coverage density ($ng\,cm^{-2}$)	588	80	400	232	258	77	74

The long alkyl chains in C18E114, C18E114-ester, and C18E45 seemed to strongly interact with the SWCNH surface, while the short alkyl chains in C10E45 and the PEG chains on both sides of E45C20E45 are supposed to weakly interact with the SWCNH surface. Moreover, an effect of the hydrophilic PEG chains on alkyl chain coverage was found in C18E114-ester, C18E114, and C18E45. The alkyl chain coverages of C18E114-ester and C18E114, which have longer PEG_{5000} chains, were lower than that of C18E45. The greater molecular volume and hydrophilicity of PEG_{5000} seemed to produce these lower alkyl chain coverage values. C18E114, with the longer PEG chain, presented a higher loading than C18E45 (Table 2). This phenomenon is consistent with a report by Hadidi et al. [38], demonstrating that LPEG with long PEG_{5000} chains were absorbed on single walled carbon nanotubes (SWCNT) much more effectively than those with short PEG_{2000} chain.

3.2. Dispersion abilities of LPEGs on SWCNHs

To compare the dispersion abilities of different LPEGs the hydrodynamic diameters of the dispersed SWCNHs were measured using DLS, and the particle sizes of the SWCNHs were plotted against the coverage values in an attempt to determine the influence of the alkyl chain coverage and PEG coverage density on dispersion of the SWCNHs (Fig. 3a and b). In general, both the alkyl chain coverage and PEG coverage density values were positively correlated with the dispersion ability. Generally speaking an alkyl chain coverage exceeding 31% or a PEG coverage density above 232 $ng\,cm^{-2}$ resulted in a small and uniform size for the SWCNHs dispersed in C-PEG, C18E114-ester, C18E114, and C18E45, while low alkyl chain coverage and PEG coverage density values led to poor dispersion of the C10E45- and E45C20E45-SWCNHs. According to the so-called "unzipping" mechanism [39], a surfactant has to penetrate the small spaces between the carbon bundles and prevent them from re-aggregating. A high LPEG coverage would result in a decrease in SWCNH aggregate agglomeration and, therefore, improve the dispersibility [40].

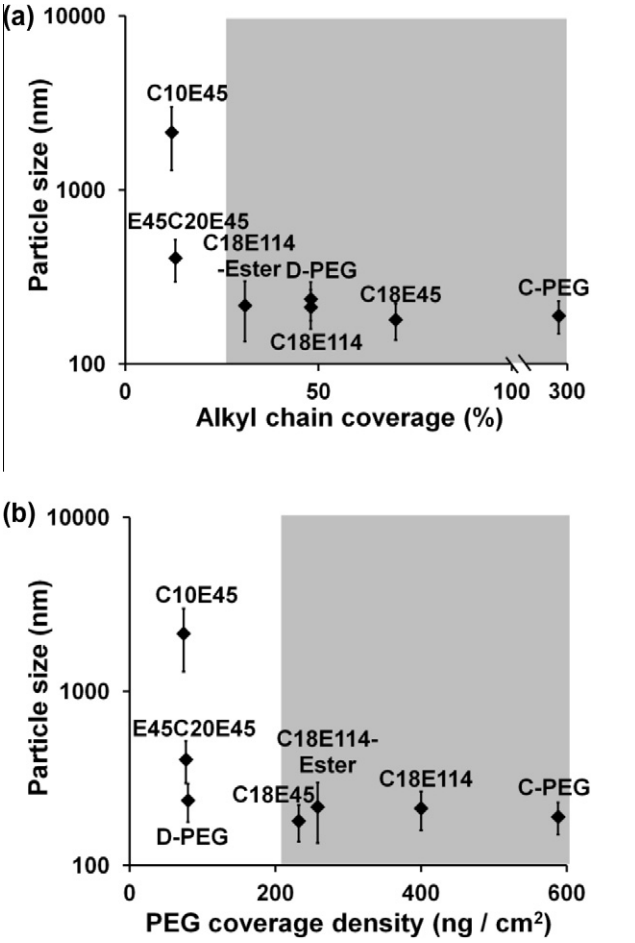

Fig. 3. Particle size of LPEG-SWCNHs in relation to (a) alkyl chain coverage and (b) PEG coverage density. Agglomerated particle sizes of SWCNHs were measured by DLS. SWCNHs were dispersed with different LPEGs at a LPEG:SWCNH weight ratio of 5:1 (means ± SD were obtained from three determinations of 87 scans, measured at 25 °C).

3.3. Dispersion stability of LPEG-SWCNH

The dispersion stability of LPEG-SWCNHs in PBS was evaluated by measuring the light transmittance at a wavelength of 700 nm for nine consecutive days. Sedimentation of the SWCNH aggregates in the dispersion yields a higher light transmittance at 700 nm, therefore, a high transmittance value indicates unstable dispersion and a low transmittance value indicates stable dispersion. Fig. 4a shows that the transmittance of the SWCNHs dispersed with C-PEG, D-PEG, C18E114, and C18E45 did not significantly change during the 9 days of observation, suggesting that these LPEGs could stably disperse SWCNHs in PBS for at least 9 days. The transmittance of the C10E45-SWCNHs dispersion in PBS increased rapidly from 34.8% to 90.1% in 3 days, while that of the C18E114-ester-SWCNHs increased dramatically to 83.0% after 5 days. The transmittance value of the E45C20E45-SWCNHs steadily increased from 16.7% to 30.3% during the 9 days of observation. For clarity Fig. 4b and c shows the relationships between the transmittance values on day 9 and the alkyl chain coverage and PEG coverage density, respectively.

Negative correlations with the transmittance values were observed for both the alkyl chain coverage and PEG coverage density (Fig. 4b and c), i.e. high values of alkyl chain coverage and PEG coverage density corresponded to low transmittance values. These results suggest that a high LPEG coverage is critical to obtain high content and stable SWCNH dispersions [41]. An alkyl chain coverage exceeding 48% or a PEG coverage density above 232 $ng\,cm^{-2}$ resulted in highly stable SWCNH dispersions, while low alkyl chain coverages and PEG coverage densities led to the poor stabilities of the C10E45- and E45C20E45-SWCNHs. The short alkyl chains in C10E45 seemed to result in detachment of C10E45 from the SWCNH surface, resulting in agglomeration and sedimentation of the SWCNHs. E45C20E45, with PEG chains on both sides of the icosanedioyl chain, also gradually detached from the SWCNH surface because of the remarkable aqueous solubility of the double

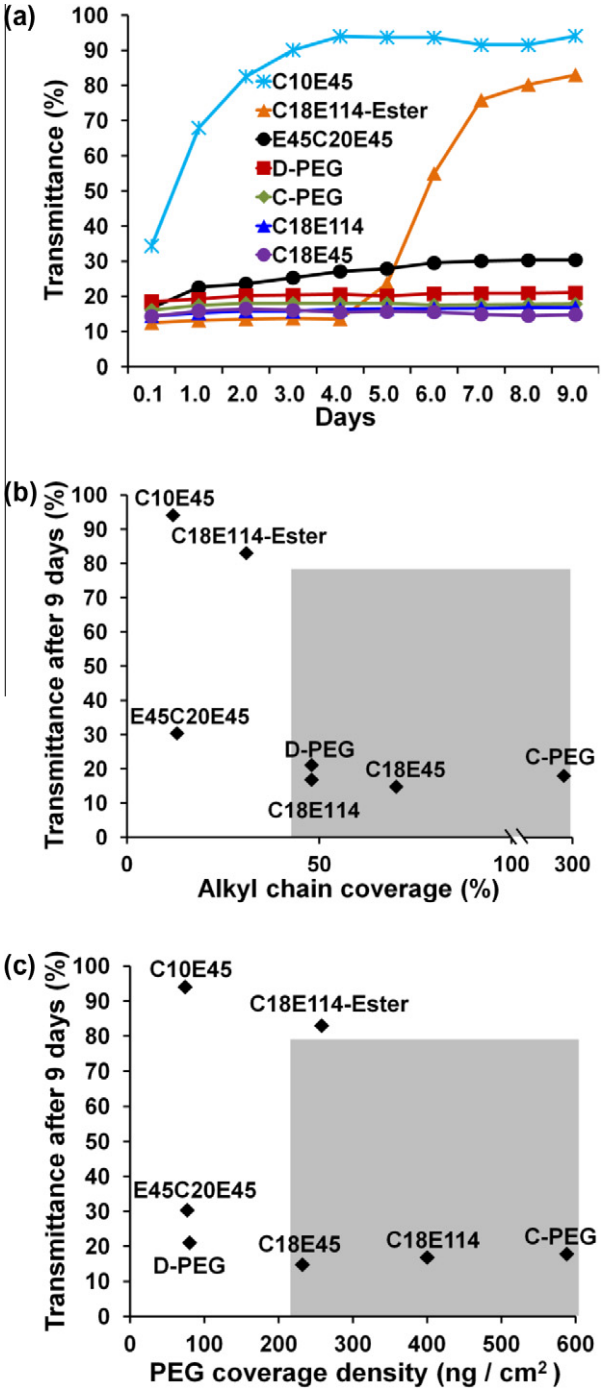

Fig. 4. Dispersion stabilities of LPEG-SWCNHs in PBS evaluated using light transmittance at a wavelength of 700 nm. Data are presented as average values of double independent experiments. (a) Time-dependent dispersion stability of LPEG-SWCNHs in PBS. The influences of (b) the alkyl chain coverage and (c) the PEG coverage density on the dispersion stabilities of the SWCNHs in PBS on day 9.

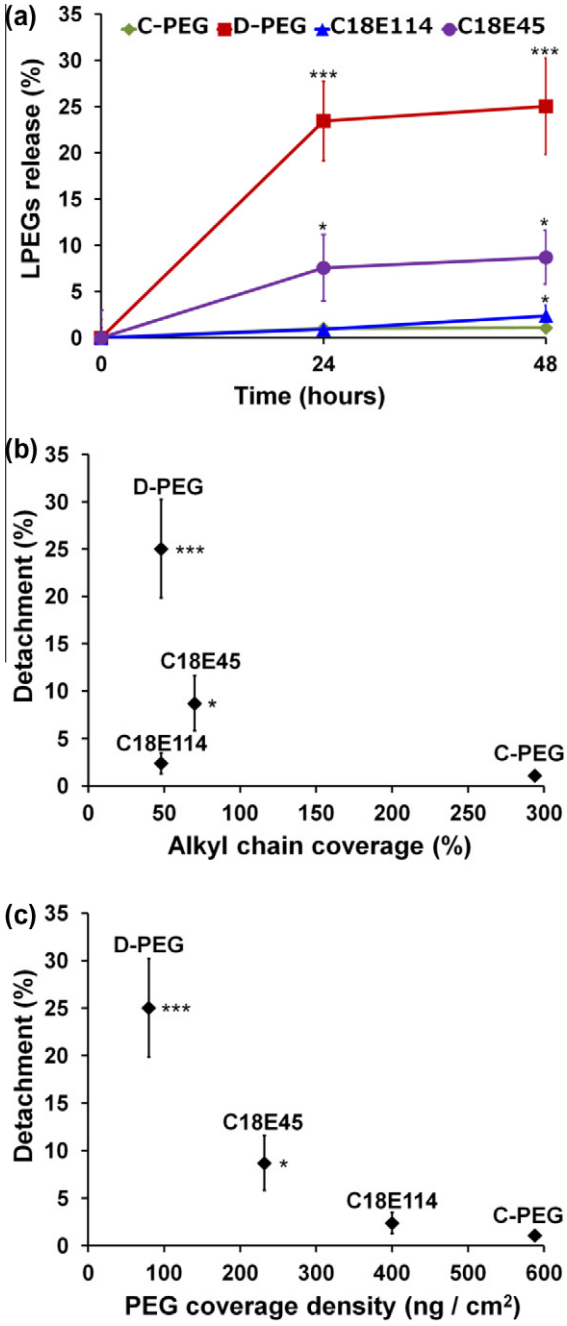

Fig. 5. (a) Time course of the cumulative detachment of LPEGs from SWCNHs in 50% bovine serum-supplemented PBS incubated at 37 °C. $^{*}P < 0.05$, $^{***}P < 0.001$ vs. 0 h data. The influences of (b) the alkyl chain coverage and (c) the PEG coverage density on the detachment of LPEGs in 50% bovine serum-supplemented PBS after incubation at 37 °C for 48 h. $^{*}P < 0.05$, $^{***}P < 0.001$ vs. CPEG. Data are expressed as the means ± SD of three independent experiments.

PEG chains. An exceptional case was C18E114-ester, which had an ester linker and may have decomposed during immersion in PBS for 9 days (see Fig. S1 in Supplementary information). Further, although D-PEG has a low PEG coverage density, which is similar to that of C10E45 and E45C20E45, a small particle size and high stability were observed (Figs. 3b and 4c). We attribute this good performance of D-PEG to the electrostatic repulsion within SWCNH particles with high negative surface charges (see Table S3 in Supplementary information) [42].

3.4. Detachment of LPEGs from SWCNHs in the presence of protein

In addition to the dispersion ability and stability in PBS, the proteins in blood may competitively exchange with LPEGs on the SWCNH surface and affect stability in the circulatory system. Therefore, high concentrations of 50% serum-supplemented PBS was used to mimic the in vivo condition. To study the detachment of LPEGs from SWCNHs in a serum-containing buffer will advance the application of SWCNHs for in vivo drug delivery and diagnosis. C-PEG, D-PEG, C18E114, and C18E45, which showed the best dispersion stabilities according to Fig. 4, were selected for the detachment studies in serum-supplemented PBS.

Fig. 5a shows that a quarter of the D-PEG was quickly detached from the SWCNHs within 24 h and C18E45 was gradually released from the SWCNHs, while little detachment of C-PEG and C18E114 was observed. Although C-PEG and D-PEG have similar alkyl chains and PEG chains, the anionic phosphate groups in D-PEG seemed to not only decrease its grafting density but also facilitate its dissociation from SWCNHs in bovine serum-supplemented PBS. A comparison of the percentage detachment relationship with alkyl chain coverage and PEG coverage density (Fig. 5b and c) shows that the PEG coverage density seems to show a better correlation with the degree of detachment than the alkyl chain coverage. A higher PEG coverage density yields less LPEG detachment. It is supposed that the proteins in serum were able to associate with the surface of the SWCNHs by replacing the LPEGs in a competitive manner [24]. A higher PEG density resulted in greater protein resistance, which meant it was harder for protein to replace the LPEGs from the SWCNHs. Other studies have also shown that a long PEG chain length and high surface density are the best conditions for protein repulsion [43]. This result suggests that the higher PEG coverage density was responsible for the lower detachment of LPEGs from the SWCNHs in biological media.

3.5. Macrophage uptake

Similar to other GNMs, it has been found that pristine SWCNHs have a tendency to mainly be taken up by the reticuloendothelial system (RES) when injected intravenously, such that they are not rapidly excreted [44]. Modification by LPEGs has been proved to be a useful and effective methodology to avoid rapid clearance of GNMs from the blood circulation by the RES [22,23]. An in vitro macrophage uptake experiment could guide us in the optimization of long circulating LPEG-SWCNHs. C-PEG, D-PEG, C18E114, and C18E45 were chosen to assay the cellular uptake by macrophage cells to clarify the influence of LPEG coverage on the uptake of LPEG-SWCNHs in vitro. The confocal images in Fig. 6a show that the dark agglomerates (SWCNHs) were mainly located within cells, and the numbers were in the order C-PEG < D-PEG < C18E114 < C18E45-SWCNHs. The cellular uptake of nanoparticles could be affected by such main factors as particle size, surface charge, and dispersing amphiphiles [30,45–50]. Because the particle sizes of these four LPEG-SWCNHs were similar in culture medium during the 2 days of observation (see Fig. S2 in Supplementary information) we attribute the different macrophage uptake to the different surface properties of LPEG-SWCNHs, such as the PEG coverage density and surface charge.

The quantities of LPEG-SWCNHs taken up were plotted against the alkyl chain coverage and PEG coverage density (Fig. 6b and c). It was found that the PEG coverage density, rather than the alkyl chain coverage, seems to correlate with macrophage uptake of the SWCNHs, except for D-PEG. This phenomenon is similar to that observed in the detachment experiment (Fig. 5). The hydrophilic PEG chain and its high surface density could inhibit replacement

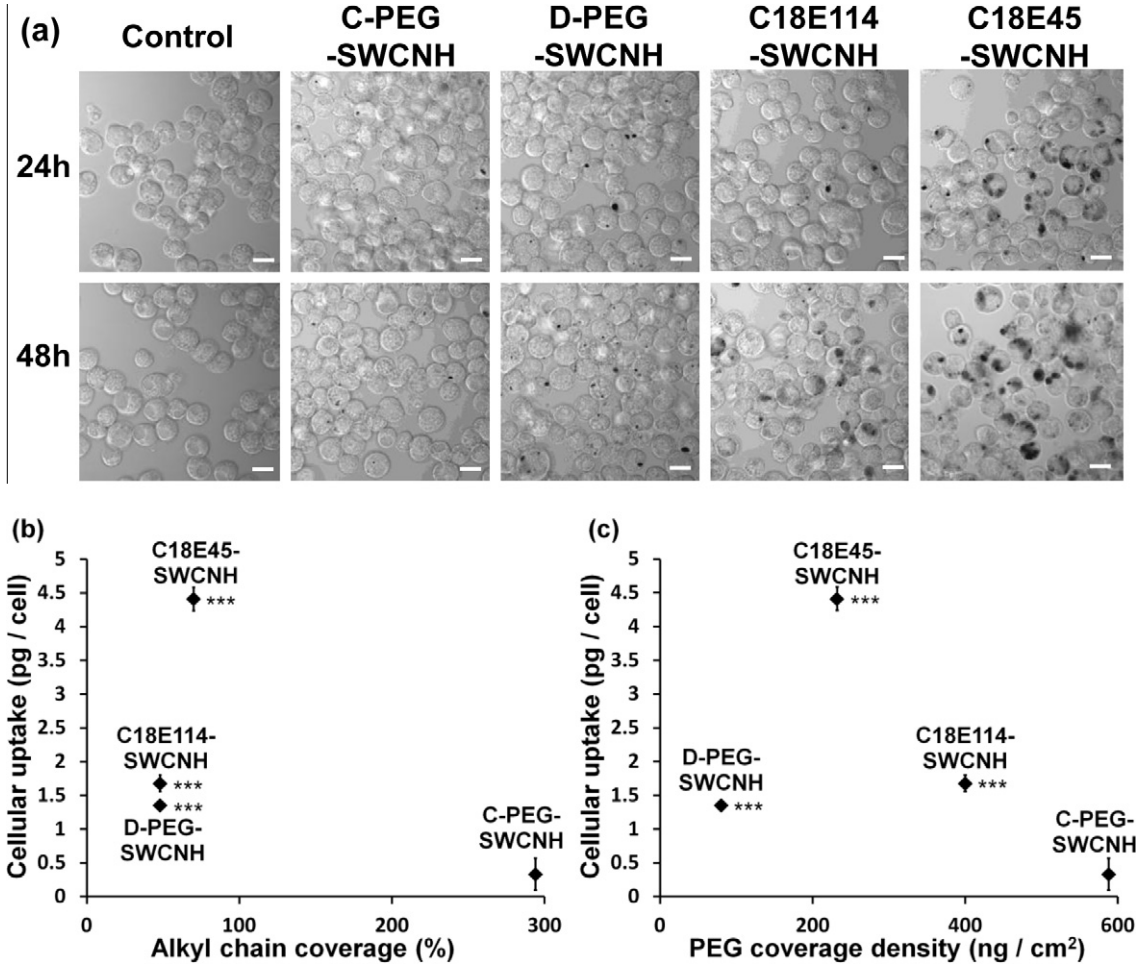

Fig. 6. (a) Microscopy images of RAW264.7 cells incubated with C-PEG, D-PEG, C18E114, and C18E45-SWCNHs (10 μg ml^{-1}) for 24 and 48 h. The black dots are the SWCNHs (scale bar in inset 10 μm). The influences of (b) the alkyl chain coverage and (c) the PEG coverage density on the cellular uptake of SWCNHs after 48 h. $^{***}P < 0.001$ vs. CPEG SWCNH. Results are expressed as the means ± SD of five independent experiments.

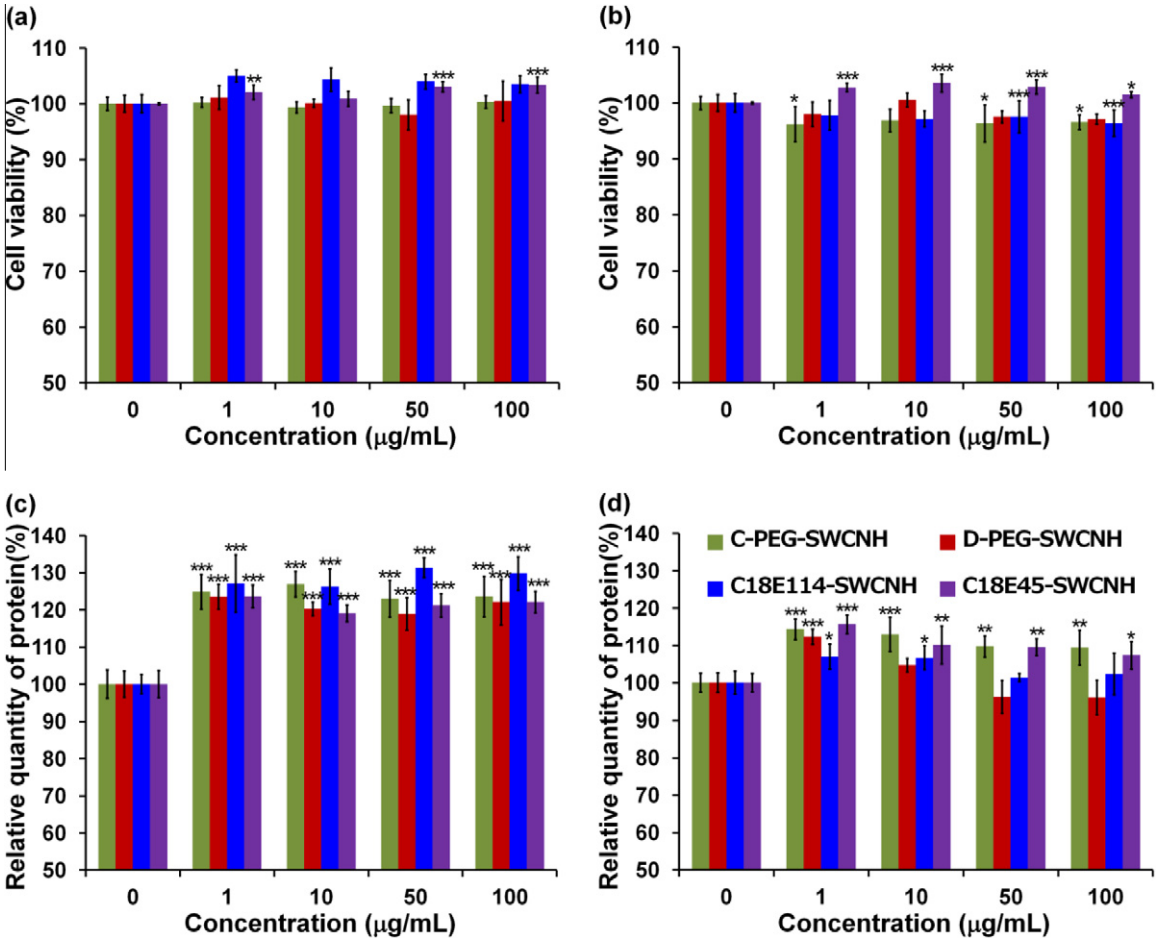

Fig. 7. Cytotoxicity of LPEG-SWCNH to RAW264.7 cells determined by WST-1 assay at (a) 24 h and (b) 48 h or by protein assay at (c) 24 h and (d) 48 h. The results are the means ± SD of the five replicated experiments. $^{*}P < 0.05$, $^{**}P < 0.01$, $^{***}P < 0.001$ vs. control (SWCNH concentration 0 μg ml^{-1}).

or binding by plasma proteins, preventing the recognition and uptake of SWCNHs by macrophages [20,21,39,51,52]. Thus a higher PEG coverage density would lead to lower macrophage uptake in the order C18E45 > C18E114 > C-PEG-SWCNH.

Although the PEG coverage density of D-PEG was the lowest, the cellular uptake was even lower than that of C18E114-SWCNHs. This could be partially explained by the strong negative zeta potential due to the anionic phosphate group in D-PEG (see Table S3 in Supplementary information). The repulsive interaction between the negatively charged cell membrane and negatively charged D-PEG-SWCNHs might inhibit the uptake of D-PEG-SWCNHs by macrophages [52,53].

3.6. Assessment of the cytotoxicity of LPEG-SWCNHs

In order to guarantee the safe use of SWCNHs for drug delivery it is necessary to provide biocompatible LPEGs for the dispersion of SWCNHs. C-PEG, D-PEG, C18E114, and C18E45, which showed the best dispersion stabilities according to Fig. 4, were selected for the cytotoxicity evaluation. The cytotoxicity of LPEG-SWCNHs to RAW264.7 cells was determined by WST-1 assay and protein assay at 24 and 48 h (Fig. 7), at dosages ranging from 1–100 μg ml^{-1} LPEG-SWCNH, which covers the commonly used doses for biological experiments, with 100 μg ml^{-1} being high enough for a toxicity test [54]. The WST-1 assay results essentially showed no cytotoxicity of LPEG-SWCNHs at both 24 and 48 h. However, after LPEG-SWCNH treatment the protein assay results demonstrated a significant increase in total protein at 24 h, even at the low concentration of 1 μg ml^{-1} SWCNH. The values of total protein dropped slightly at 48 h. These phenomena suggest that LPEG-SWCNHs have an essentially low toxicity to macrophages [55,56], but may be able to temporally activate macrophages [54,57]. Activation of macrophages by SWCNHs is an ongoing area of research.

4. Conclusion

We have demonstrated the effects of alkyl chain coverage and PEG coverage density on the dispersion ability, dispersion stability, and detachment of LPEGs from SWCNHs, and macrophage uptake of LPEG-SWCNHs. An alkyl chain coverage or PEG coverage density higher than a certain value could finely disperse the SWCNHs for a long period of time. Moreover, an increased PEG coverage density resulted in less detachment of LPEGs from SWCNHs, and a high coverage density of hydrophilic PEG chains was effective in preventing the uptake of SWCNHs by macrophages. The anionic phosphate linker was a double-edged sword. It induced a lower alkyl chain coverage and PEG coverage density on SWCNHs and accelerated the detachment of LPEGs from SWCNHs, especially in bovine serum-supplemented PBS. On the other hand, once D-PEG attached to the surface of SWCNHs the high negative surface charge of D-PEG SWCNH ensured good dispersibility and the electrical repulsive force between the anionic phosphate groups and the negatively charged cell surfaces was partially responsible for the lower uptake of D-PEG-SWCNH by macrophages, which would be favorable in preventing the uptake of SWCNHs by the RES in future

drug delivery applications. These results could serve as a guide for the design of suitable LPEGs for the dispersion and functionalization of GNMs, especially for biomedical applications.

Acknowledgements

M.Y. and S.I. acknowledge financial support received from the Balzan Foundation. This work was partly supported by a Grant-in-Aid for Scientific Research (A) (No. 23241037).

Appendix A. Figures with essential colour discrimination

Certain figures in this article, particularly Figs. 2, 4, 5 and 7, are difficult to interpret in black and white. The full colour images can be found in the on-line version, at http://dx.doi.org/10.1016/j.actbio.2012.09.012.

Appendix B. Supplementary data

Supplementary data associated with this article can be found, in the online version, at http://dx.doi.org/10.1016/j.actbio.2012.09.012.

References

[1] Singh R, Nalwa HS. Medical applications of nanoparticles in biological imaging, cell labeling, antimicrobial agents, and anticancer nanodrugs. J Biomed Nanotechnol 2011;7:489–503.
[2] Scheinberg DA, Villa CH, Escorcis FE, McDevitt MR. Conscribes of the infinite armada: systematic cancer therapy using nanomaterials. Nat Rev Clin Oncol 2010;7:266–76.
[3] Feng L, Liu Z. Graphene in biomedicine: opportunities and challenges. Nanomedicine (Lond) 2011;6:317–24.
[4] Bekyarova E, Ni Y, Malarkey EB, Montana V, McWilliams JL, Haddon RC, et al. Applications of carbon nanotubes in biotechnology and biomedicine. J Biomed Nanotechnol 2005;1:3–17.
[5] Bottini M, Rosato N, Bottini N. PEG-modified carbon nanotubes in biomedicine: current status and challenges ahead. Biomacromolecules 2011;12:3381–93.
[6] Ajima K, Yudasaka M, Murakami T, Maigné A, Shiba K, Iijima S. Carbon nanohorns as anticancer drug carriers. Mol Pharm 2005;2:475–80.
[7] Fu K, Sun YP. Dispersion and solubilization of carbon nanotubes. J Nanosci Nanotechnol 2003;3:351–64.
[8] Hirsch A. Functionalization of single-walled carbon nanotubes. Angew Chem Int Ed Engl 2002;41:1853–9.
[9] Fu K, Huang W, Lin Y, Riddle LA, Carroll DL, Sun YP. Defunctionalization of functionalized carbon nanotubes. Nano Lett 2001;1:439–41.
[10] Zhao B, Hu H, Yu A, Perea D, Haddon RC. Synthesis and characterization of water soluble single-walled carbon nanotube graft copolymers. J Am Chem Soc 2005;127:8197–203.
[11] Sinani VA, Gheith MK, Yaroslavov AA, Rakhnyanskaya AA, Sun K, Mamedov AA, et al. Aqueous dispersions of single-wall and multiwall carbon nanotubes with designed amphiphilic polycations. J Am Chem Soc 2005;127:3463–72.
[12] Zheng M, Jagota A, Semke ED, Diner BA, McLean RS, Lustig SR, et al. DNA-assisted dispersion and separation of carbon nanotubes. Nat Mater 2003;2:338–42.
[13] Huang W, Taylor S, Fu K, Lin Y, Zhang D, Hanks TW, et al. Attaching proteins to carbon nanotubes via diimide-activated amidation. Nano Lett 2002;2:311–4.
[14] Wang R, Cherukuri P, Duque JG, Leeuw TK, Lackey MK, Moran CH, et al. SWCNT PEG-eggs: single-walled carbon nanotubes in biocompatible shell-crosslinked micelles. Carbon 2007;45:2388–93.
[15] Lee JU, Huh J, Kim KH, Park C, Jo WH. Aqueous suspension of carbon nanotubes via non-covalent functionalization with oligothiophene-terminated poly(ethylene glycol). Carbon 2007;45:1051–7.
[16] Matsumura S, Sato S, Yudasaka M, Tomida A, Tsuruo T, Iijima S, et al. Prevention of carbon nanohorn agglomeration using a conjugate composed of comb-shaped polyethylene glycol and a peptide aptamer. Mol Pharm 2009;6:441–7.
[17] Murakami T, Sawada H, Tamura G, Yudasaka M, Iijima S, Tsuchida K. Water-dispersed single-wall carbon nanohorns as drug carriers for local cancer chemotherapy. Nanomedicine (Lond) 2008;3:453–63.
[18] Liu Z, Fan AC, Rakhra K, Sherlock S, Goodwin A, Chen X, et al. Supramolecular stacking of doxorubicin on carbon nanotubes for in vivo cancer therapy. Angew Chem Int Ed Engl 2009;48:7668–72.
[19] Xu J, Iijima S, Yudasaka M. Appropriate PEG compounds for dispersion of single wall carbon nanohorns in salted aqueous solution. Appl Phys A 2010;99:15–21.
[20] Romberg B, Hennink WE, Storm G. Sheddable coating for long-circulating nanoparticles. Pharm Res 2008;25:55–71.
[21] Vonarbourg A, Passirani C, Saulnier P, Benoit JP. Parameters influencing the stealthiness of colloidal drug delivery systems. Biomaterials 2006;27:4356–73.
[22] Liu X, Tao H, Yang K, Zhang S, Lee ST, Liu Z. Optimaization of surface chemistry on single-walled carbon nanotubes for in vivo photothermal ablation of tumors. Biomaterials 2011;32:144–51.
[23] Liu Z, Davis C, Cai W, He L, Chen X, Dai H. Circulation and long-term fate of functionalized, biocompatible single-walled carbon nanotubes in mice probed by Raman spectroscopy. Proc Natl Acad Sci USA 2008;105:1410–5.
[24] Cherukuri P, Gannon CJ, Leeuw TK, Schmidt HK, Smalley RE, Curley SA, et al. Mammalian pharmacokinetics of carbon nanotubes using intrinsic near-infrared fluorescence. Proc Natl Acad Sci USA 2006;103:18882–6.
[25] Patel HM, Moghimi SM. Serum-mediated recognition of liposomes by phagocytic cells of the reticuloendothelial system – the concept of tissue specificity. Adv Drug Deliv Rev 1998;32:45–60.
[26] Iijima S, Yudasaka M, Yamada R, Bandow S, Suenaga K, Kokai F, et al. Nano-aggregates of single-walled graphitic carbon nano-horns. Chem Phys Lett 1999;309:165–70.
[27] Utsumi S, Miyawaki J, Tanaka H, Hattori Y, Ito T, Ichikuni N, et al. Opening mechanism of internal nanoporosity of single-wall carbon nanohorn. J Phys Chem B 2005;109:14319–24.
[28] Fan J, Yudasaka M, Miyawaki J, Ajima K, Murata K, Iijima S. Control of hole opening in single-wall cabon nanotubes and single-wall carbon nanohorns using oxygen. J Phys Chem B 2006;110:1587–91.
[29] Jia Z, Tian C. Quantitative determination of polyethylene glycol with modified Dragendorff reagent method. Desalination 2009;247:423–9.
[30] Zhang M, Zhou X, Iijima S, Yudasaka M. Small-sized carbon nanohorns enabling cellular uptake control. Small 2012;8:2524–31.
[31] Richard C, Balavoine F, Schultz P, Ebbesen TW, Mioskowski C. Supramolecular self-assembly of lipid derivatives on carbon nanotubes. Science 2003;300:775–8.
[32] Diama A, Matthies B, Herwig KW, Hansen FY, Criswell L, Mo H, et al. Structure and phase transitions of monolayers of intermediate-length n-alkanes on graphite studied by neutron diffraction and molecular dynamics simulation. J Chem Phys 2009;131:84707.
[33] Herwig KW, Matthies B, Taub H. Solvent effects on the monolayer structure of long n-alkane molecules adsorbed on graphite. Phys Rev Lett 1995;75:3154–7.
[34] Hibino M, Sumi A, Hatta I. Molecular arrangements of fatty acids and cholesterol at liquid/graphite interface observed by scanning tunneling microscopy. Jpn J Appl Phys 1995;34:3354–9.
[35] Murata K, Kaneko K, Kokai F, Takahashi K, Yudasaka M, Iijima S. Pore structure of single-wall carbon nanohorn aggregates. Chem Phys Lett 2000;331:14–20.
[36] O'Connell MJ, Boul P, Ericson LM, Huffman C, Wang Y, Haroz E, et al. Reversible water-solubilization of single-walled carbon nanotubes by polymer wrapping. Chem Phys Lett 2001;342:265–71.
[37] Niyogi S, Densmore CG, Doorn SK. Electrolyte tuning of surfactant interfacial behavior for enhanced density-based separations of single-walled carbon nanotubes. J Am Chem Soc 2009;131:1144–53.
[38] Hadidi N, Kobarfard F, Nafissi-Varcheh N, Aboofazeli R. Optimization of single-walled carbon nanotube solubility by noncovalent PEGylation using experimental design methods. Int J Nanomed 2011;6:737–46.
[39] Strano MS, Moore VC, Miller MK, Allen MJ, Haroz EH, Kittrell C, et al. The role of surfactant adsorption during ultrasonication in the dispersion of single-walled carbon nanotubes. J Nanosci Nanotechnol 2003;3:81–6.
[40] Vaisman L, Wagner HD, Marom G. The role of surfactants in dispersion of carbon nanotubes. Adv Colloid Interf Sci 2006;128–130:37–46.
[41] Heister E, Lamprecht C, Neves V, Tîlmaciu C, Datas L, Flahaut E, et al. Higher dispersion efficacy of functionalized carbon nanotubes in chemical and biological environments. ACS Nano 2010;4:2615–26.
[42] Vaisman L, Marom G, Wagner HD. Dispersions of surface-modified carbon nanotubes in water-soluble and water-insoluble polymers. Adv Funct Mater 2006;16:357–63.
[43] Jeon SI, Lee JH, Andrade JD, De Gennes PG. Protein–surface interactions in the presence of polyethylene oxide. I. Simplified theory. J Colloid Interf Sci 1991;142:149–58.
[44] Miyawaki J, Matsumura S, Yuge R, Murakami T, Sato S, Tomida A, et al. Biodistribution and ultrastructural localization of single-walled carbon nanohorns determined in vivo with embedded Gd_2O_3 labels. ACS Nano 2009;3:1399–406.
[45] Jin H, Heller DA, Sharma R, Strano MS. Size-dependent cellular uptake and expulsion of single-walled carbon nanotubes: single particle tracking and a generic uptake model for nanoparticles. ACS Nano 2009;3:149–58.
[46] Raffa V, Ciofani G, Vittorio O, Riggio C, Cuschieri A. Physicochemical properties affecting cellular uptake of carbon nanotubes. Nanomedicine (Lond) 2010;5:89–97.
[47] Antonelli A, Serafini S, Menotta M, Sfara C, Pierigé F, Giorgi L, et al. Improved cellular uptake of functionalized single-walled carbon nanotubes. Nanotechnology 2010;21:425101.
[48] Chen L, Mccrate JM, Lee JC, Li H. The role of surface charge on the uptake and biocompatibility of hydroxyapatite nanoparticles with osteoblast cells. Nanotechnology 2011;22:105708.
[49] Iverson NM, Sparks SM, Demirdirek B, Uhrich KE, Moghe PV. Controllable inbibition of cellular uptake of oxidized low-density lipotrotein: structure–function relationships for nanoscale amphiphilic polymers. Acta Biomater 2010;6:3081–91.
[50] Zhao F, Zhao Y, Liu Y, Chang X, Chen C, Zhao Y. Cellular uptake, intracellular trafficking, and cytotoxicity of nanomaterials. Small 2011;7:1322–37.

[51] Gref R, Domb A, Quellec P, Blunk T, Müller RH, Verbavatz JM, et al. The controlled intravenous delivery of drugs using PEG-coated sterically stabilized nanospheres. Adv Drug Deliv Rev 1995;16:215–33.
[52] Alexis F, Pridgen E, Molnar LK, Farokhzad OC. Factors affecting the clearance and biodistribution of polymeric nanoparticles. Mol Pharm 2008;5:505–15.
[53] He C, Hu Y, Yin L, Tang C, Yin C. Effects of particle size and surface charge on cellular uptake and biodistribution of polymeric nanoparticles. Biomaterials 2010;31:3657–66.
[54] Cheng WW, Lin ZQ, Wei B-F, Zen Q, Han B, Wei C-X, et al. Single-walled carbon nanotube induction of rat aortic endothelial cell apoptosis: reactive oxygen species are involved in the mitochondrial pathway. Int J Biochem Cell Biol 2011;43:564–72.
[55] Pulskamp K, Diabaté S, Krug HF. Carbon nanotubes show no sign of acute toxicity but induce intracellular reactive oxygen species in dependence on contaminants. Toxicol Lett 2007;168:58–74.
[56] Fiorito S, Serafino A, Andreola F, Bernier P. Effects of fullerenes and single-wall carbon nanotubes on murine and human macrophages. Carbon 2006;44:1100–5.
[57] Dumortier H, Lacotte S, Pastorin G, Marega R, Wu W, Bonifazi D, et al. Functionalized carbon nanotubes are non-cytotoxic and preserve the functionality of primary immune cells. Nano Lett 2006;6:1522–8.